SAND2000-2364 J

BENT-BEAM ELECTROTHERMAL ACTUATORS: LINEAR AND ROTARY MICROENGINES

Jae-Sung Park, Larry L. Chu, Andrew D. Oliver*, and Yogesh B. Gianchandani[1]
University of Wisconsin, Madison, USA
*Sandia National Laboratories, New Mexico, USA

ABSTRACT

This paper reports on the use of bent-beam electrothermal actuators for the purpose of generating rotary and long-throw rectilinear displacements. The rotary displacements were achieved by orthogonally arranged pairs of cascaded actuators that were used to rotate a gear. Devices were fabricated using electroplated Ni, p^{++} Si, and polysilicon as structural materials. Displacements of 20-30 μm with loading forces >150 μN at actuation voltages <12 V and power dissipation <300 mW could be achieved in the orthogonally arranged actuator pairs. A design that occupied <1 mm^2 area was demonstrated. The long-throw rectilinear displacements were achieved by inchworm mechanisms in which pairs of opposing actuators grip and shift a central shank that is cantilevered on a flexible suspension. A retractable passive lock holds the displaced shank between pushes and when the power is off. This arrangement permits large output forces to be developed at large displacements, and requires zero standby power. Several designs were fabricated using electroplated Ni as the structural material. Displacements >100 μm at forces >200 μN were measured.

[1] Corresponding author: 1415 Engineering Dr., UW-Madison, 53706-1691, USA; Tel: (608)262-2233; Fax: 262-1267; yogesh@engr.wisc.edu

DISCLAIMER

I. INTRODUCTION

Although many micromachined actuators have been developed in the past, the options for micromachining processes which use Si as the structural material are limited to electrostatic and electrothermal devices. Electrothermal actuators consume more power than electrostatic ones, but they provide higher forces and can generally be driven with lower voltages, allowing standard interface electronics to be used. Amongst electrothermal devices that provide in-plane motion, bent beam actuators offer an attractive compromise of displacement, force, scalability and simplicity in design [1-3].

Typical manifestations of bent-beam electrothermal actuators are illustrated in Fig. 1. In the simplest version, an electric current is passed though a V-shaped beam that is anchored at its ends, and thermal expansion caused by joule heating pushes the apex outward. The beams may be cascaded for larger displacement: if two primary base units are driven by the same power supply, there will be essentially zero current sustained by the secondary unit, which then serves only as a mechanical amplifier of the displacement. Cascaded devices have 3x-4x larger displacements than simple beams.

Polysilicon, p^{++} Si, and electroplated Ni are commonly used structural materials for MEMS, and are good candidates for electro-thermal actuators. Materials that can withstand elevated actuation temperatures and those that have a high coefficient of thermal expansion are attractive for large displacements. In addition, if the expansion coefficient of the structure is the same as that of the substrate, the position of the actuator will not vary with changes in ambient temperature. Since the natural thermal isolation of most microstructures with respect to the substrate and the ambient is 1,000-10,000 K/W in air, maintaining a temperature of 600°C requires only 60-600 mW of power [2]. Moreover, the actuation voltages are generally <25 V, permitting the use of standard electronic interfaces that are generally inadequate for electrostatic actuators. Reliability studies of p^{++} Si bent-beam actuators have shown that devices can be operated for >30 million cycles without amplitude degradation [4].

This paper reports on rotary and rectilinear microengines that utilize the time-sequenced operation of bent-beam electrothermal actuators [5]. The rotary engines, which utilize two orthogonally placed actuators, are described in section II. The rectilinear engines, which utilize two actuators and a mechanical lock in a grip-and-shift inchworm mechanism, are described in section III. The inchworms offer long throw and high force with zero standby power consumption.

II. ROTARY MICROENGINE

Electrostatically driven rotary actuators have been developed for use in micromechanical discriminators for secure systems [6] as well as a variety of micro-optical component such as scanners and switches [7-9]. In applications for which the loading forces are relatively small (<50 μN), surface micromachined electrostatic actuators can be driven with voltages in the range of 50-100 V. When higher output forces are necessary or when lower driving voltages are required, electrothermal drives may offer a reasonable compromise.

The rectilinear stroke of the bent-beam actuator can be converted into rotary motion of a gear by repeated tangential impact [10] or by orthogonally placed linear actuators acting in tandem [6]. The latter alternative provides continuous application of force and can be easily implemented by an orthogonal arrangement of two electrothermal actuators. The time-sequenced operation of this mechanism provides the motion necessary to rotate the output gear. It may also be used as a general-purpose 2-D positioner in the plane of the structure.

In order to meet the performance target for this effort, the rotary actuator must drive a 100 μm diameter gear with a stall torque of at least 500 pN-m, using a drive voltage <20 V. Since the loading force is small, the motivation for electro-thermal actuation in this context is largely the lower actuation voltages which permit the used of standard circuit interfaces. As shown in Fig. 2, with the drive pin located 17 μm from the center of the gear, the target displacement for the actuators is about 34 μm. The 500 pN-m stall torque requirement is satisfied if the output force at this displacement exceeds 29 μN.

The finite element analysis (FEA) of orthogonal pairs of identical cascaded actuators shows that a 30 μm stroke is achievable in Si with suspension lengths of ≈600 μm at <500°C (Fig. 3). This FEA model included both the X and Y actuators, and accounted for the loading of each upon the other (which is larger than 29 μN output load). Although shallower bending angles promise higher displacement, they have a greater propensity for out-of-plane buckling.

Buckling

In many cases, out-of-plane buckling can be the limiting factor for maximum displacement, output force, and drive temperature of an actuator. For cascaded structures and other complex shapes, FEA was used to examine stability. The buckling conditions of the structures were determined under an externally applied loading force of 40 μN, which included the maximum specified loading force of 29 μN as well as an 11 μN safety margin. The predictions for buckling temperature obtained by FEA were pessimistic because only one degree of freedom was specified. In reality, in-plane deflections that occur in normal operation of the device reduce the propensity for out-of-plane buckling. It is also helpful to evaluate the conditions for in-plane buckling. When in-plane buckling occurs, the V-shape of the base unit in a cascaded device becomes inverted, rendering the device inoperational. Figure 4(a) shows the temperature at which an actuator will buckle out-of-plane, whereas Fig. 4(b) shows the maximum lateral deflection that can be achieved before a cascaded actuator buckles in-plane. Bending angles of $\theta 1$=0.1 rad. and $\theta 2$=0.2 rad. provide the best compromise between large displacement and both in-plane and out-of-plane buckling. Process variations such as greater structural thickness or longitudinal corrugations in the structural material can help to further increase the out-of-plane buckling temperature.

Fabrication and Measurement Results

The operation of the orthogonal drive was first validated by fabricating it without the output gear, as shown in Fig. 5. Samples were fabricated in both electroplated Ni and p^{++} Si using abbreviated process sequences which provided a single structural layer. The loading of the gear on the actuator was emulated by a loading beam constrained by brackets at each end (Fig. 6). This

beam was attached transversely to the drive shaft along each axis and/or at the location of the gear (Fig. 5).

A number of different designs were fabricated with dimensional variables as listed in Table I. The measured results are plotted in Fig. 7. For devices R3 and RJ3, there was no loading force applied, whereas for devices R5 and R6, loading force was applied only for displacement higher than a certain threshold, which was the displacement necessary for the loading beam to come into contact with its bracket constraint. Beyond this threshold, the loading force increased with displacement, which was measured using integrated verniers. The p^{++} Si devices with beam lengths of 500-1000 μm showed displacements of 20-30 μm when symmetrically driven at total power levels <300 mW, and peak actuation voltages in the 6-8 V range. An electroplated Ni device with 500 μm beam length and 11 μm thickness provided 15 μm displacement at 0.8 V, and 450 mW. When a single axis is actuated, a backward displacement of about 1 μm occurs along the complementary axis (Fig. 8). This is easily compensated by activating the complementary actuator.

A modified version of the orthogonal drive that occupies <1 mm^2 less area is shown in Fig. 9. The X drive was comprised of two parallel primary bent-beams with L1=600 μm, W=3.7 μm, θ=0.1 rad. The secondary beam, which was attached to the apices of the primary beams at one end and anchored at the other end, had L2=600 μm, W2=3.7 μm, and θ2=0.1 rad. The Y drive was an ordinary cascaded device with L1=L2=600 μm, W1=5.7 μm, W2=3.7 μm, θ1=0.1 rad., and θ2=0.2 rad. The beams were 4.25 μm thick. The beams at both ends of the drive shaft and at the base of the secondary element in the Y-drive were narrowed to 1.7 μm width for a 40 μm segment in order to make the structure more compliant. The segments of these beams that overlap the gears were 2.25 μm thick, while the gears were 2.5 μm thick. The device was fabricated using polysilicon as the structural material in the Sandia SUMMiT IV™ process.

The measured response of an isolated and unloaded instance of the cascaded polysilicon Y-drive is shown in Fig. 10. The peak displacement achieved was about 33.4 μm at 14.4 V and 375 mW. The operation of the microengine is shown in the optical micrographs of Fig. 11, which show the drive pin located in each quadrant as it rotated around the gear hub. The on-off sequence of each drive is annotated in the figure. The peak voltage and current for the X-drive were 11.9 V and 17.9 mA, respectively; for the Y-drive, they were 9.6 V and 24.0 mA. A square wave signal which provided 50 ms in each quadrant was used to rotate the gear at 300 rpm. Measurements indicate that the –3 dB bandwidth for the displacement of the bent-beam electrothermal actuators is about 1 KHz [4]. This suggests that with proper timing and control, it may be possible to rotate the gears at about 15,000 rpm.

The devices were operated in air for >15 minutes. The primary failure mode was the separation of the hub from the substrate, while secondary failure mode was the breaking of the pivot from the output gear. Both modes were probably related to the large forces applied by the electrothermal actuators; they are not commonly observed when electrostatic actuators, which provide much lower forces, are used to drive the same gears. Better control of the drive timing and larger feature sizes at the high stress points can alleviate this problem in future efforts. Another option is to use complaint microtransmissions, which can tailor the force-displacement relationship as required [11].

III. INCHWORM TYPE MICROENGINE

In the preceding section, bent-beam actuators with one level of cascading were shown to generate rectilinear displacements of tens of microns. For applications that require an order of magnitude more displacement, alternate approaches are necessary. Since rotary actuators are available, one option is to use gear trains coupled to a linear rack. Another option, which is potentially less susceptible to frictional wear, is to use inchworms. Pairs of opposing bent-beam actuators are pulsed to grip and shift a central shank, which is cantilevered on a flexible suspension (Fig. 12). The sidewall of the shank and the mating surfaces of the actuators are corrugated to

reduce their reliance on friction to hold the displacement against large forces. The actuators effectively work as a *split cascade*: when actuated, the individual actuators move forward until they touch the shank, at which point they effectively form a single actuator with an additional level of cascading. Another pair of opposing actuators, located at a different point along the shank, can be actively operated out of phase with the first to provide complementary motion. Alternatively, the second pair can serve as a passive lock that prevents the shank from being pulled back once it has been displaced. The concept of the passive lock is illustrated in Fig 12(a): cantilevers placed at an angle lateral to the shank come into contact with it as the shank advances. The angle of their placement and the design of the corrugated mating surfaces is such that they offer little resistance to a forward displacement of the shank, which tends to disengage them from the teeth along its sides. Conversely, a reverse displacement of the shank tends to engage the intermeshed teeth, preventing it from being pulled back. The cantilevers may be optionally attached to actuators so that they may be retracted, as shown in Fig. 12(b). This results in tremendous power savings when a displacement must be held for extended time intervals. The incremental displacement of the shank is governed by the pitch of the corrugation on the shank and the face of the lock. The maximum displacement of the shank is reached when the pull-back force from the extension of the spring and the drag from the locking mechanism match the output force from the active pair of actuators. This inchworm mechanism contrasts with impact-driven slider mechanisms, which do not apply a continuous force to the displaced element [12,13].

Fabrication and Measurement Results

A number of different inchworms were designed and fabricated using a single structural layer of electroplated Ni. Preliminary tests were performed on five designs listed in Table II. Three of these, including I11, I33, and IL1 are shown in Figs. 13 and 14. Not shown are I100, which is similar to I33 but has a different spring, and IL4, which is similar to IL1 but has 40% longer beams, and releasable locks. Designs I11, I33, and I100 use pairs of simple actuators that effectively have a one-level cascade when they touch the shank, whereas designs IL1 and IL4 have

a two-level cascade after they touch the shank. Designs I11 and IL4 have releasable passive locks, whereas the other have unreleasable ones.

The preliminary measurement results are summarized in Table II. Locked displacements of up to 104 μm were achieved using DC (≤1 V, 250 mA) or pulsed (≤1.2 V, ≤600 mA) actuation. The best pulse widths were empirically found to be in the 20-40 ms range. Each pulse advanced the shank by an integral multiple of 8 μm, which was the pitch of the corrugation along the sides of the shank. As shown in a close-up in Fig. 14, the lock holds the displacement when the power is turned off and the actuator is retracted.

The stiffness of the spring located at the base of each inchworm shank can be estimated from measured dimensional parameters by the formula $K_{sp}=192EI_s/(NL_s^3)$, where E is the Young's modulus of the electroplated Ni, estimated to be 150 GPa; I_s is the moment of inertia of the spring beam, which is a half loop; L_s is the length of the half loop, and N is the total number of them present. This formula assumes fixed boundary conditions at the location of the fold in each loop, which matches observations of fabricated springs. Using this, the peak forces generated in devices I100 and IL1 were calculated as 171 μN and 204 μN, respectively (Table II). In reality, the maximum displacement achievable by the inchworm is limited not only by spring stiffness, but also by out-of-plane deformation of the actuators or the shank. These are caused by stress gradients in the structural material and by forcing together the sloping sidewalls of the shank and the mating surfaces of the actuators. These problems can be solved by an improved fabrication process, which would result in peak output forces and displacements that are greater than the measurements listed in Table II. Another option is to add out-of-plane constraints using an additional structural layer.

V. CONCLUSION

This effort has explored microengines based on bent-beam suspensions for the purpose of generating rotary and rectilinear displacements. Several different structural materials were evaluated, including electroplated Ni, bulk micromachined p^{++} Si, and surface micromachined

polysilicon. Orthogonally placed pairs of cascaded thermal actuators which essentially formed 2-D positioners were applied to rotary drives. Structures fabricated from p^{++} Si with 500-1000 μm beam lengths and 6.5 μm thickness showed 20-30 μm diagonal displacement with >150 μN loading at actuation levels of 6-8 V, and 250-300 mW. An electroplated Ni structure with 500 μm beam lengths and 1.1 μm thickness provided 15 μm displacement at 0.8 V, 450 mW. A modified rotary engine that occupied <1 mm^2 area was formed by dropping one of the primary beams in the orthogonal pair of cascaded actuators. It was fabricated using surface micromachined polysilicon with beams of 600 μm length and 4.25 μm thickness, and used to drive a gear with actuation voltages below 12 V.

Opposing pairs of simple and cascaded actuators were applied to inchworms. Several designs were fabricated with electroplated Ni, and tested with DC and pulsed actuation schemes. Devices with 500-1500 μm beam lengths and 8-14 μm thickness provided displacements up to 104 μm against estimated loading forces upto 204 μN. Passive locks allowed the standby power to be reduced to zero. Overall, these efforts have demonstrated that bent-beam electro-thermal actuators can be used to generate non-resonant displacements and forces in the 100 μm, 100 μN range, and can be used in energy efficient ways for a variety of applications.

ACKNOWLEDGEMENTS

The authors thank Mr. Ekapon Siwapornsathain and Ms. Lisa Otradovec for help with testing of the inchworms and rotary actuators, respectively. Partial funding for the effort on rotary actuators was provided by Sandia National Labs. The support of Mr. David Plummer is greatly appreciated. Sandia is a multi-program laboratory operated by Sandia Corporation, a Lockheed Martin Company, for the United States Department of Energy under contract DE-AC04-94AL85000. Additional support was provided by an NSF Career Award to an author (YBG).

REFERENCES

[1] H. Guckel, J. Klein, T. Christenson, K. Skrobis, M. Laudon, E.G. Lovell, "Thermo-magnetic metal flexure actuators," *Solid-State Sensor & Actuator Workshop (Hilton Head),* pp. 73-75, June 1992

[2] L. Que, J.-S. Park, Y.B. Gianchandani, "Bent-Beam Electro-Thermal Actuators for High Force Applications," *IEEE Conf. on Micro Electro Mechanical Systems,* pp. 31-36, Jan. 1999, Orlando (a journal paper based on this work has been submitted to *JMEMS*)

[3] J. Jonsmann, O. Sigmund, S. Bouwstra, "Compliant Electro-Thermal Microactuators," *IEEE Conf. on Micro Electro Mechanical Systems,* Orlando, pp. 588-592, Jan. 1999

[4] L. Que, J.-S. Park, M.-H. Li, and Y. Gianchandani, "Reliability Studies of Bent-Beam Electro-Thermal Actuators," *IEEE International Reliability Physics Symposium (IRPS00),* San Jose, California, Apr. '00

[5] J.-S. Park, L.L Chu, E. Siwapornsathain, A.D. Oliver, and Y. Gianchandani, "Long Throw and Rotary Output Electro-Thermal Actuators Based on Bent-Beam Suspensions," *IEEE International Conference on Micro Electro Mechanical Systems (MEMS00),* pp. 680-685, Miyazaki, Japan, Jan. '00

[6] M.S. Rodgers, J.J. Sniegowski, "Five-level polysilicon surface micromachining technology: application to complex micromechanical systems," *Solid-State Sensor & Actuator Workshop (Hilton Head),* pp. 144-149, June 1998

[7] E.J. Garcia, "Micro-flex mirror and instability actuation technique," *IEEE Conf. on Micro Electro Mechanical Systems,* Heidelberg, pp. 470-5, Jan. 1998

[8] A.A. Yasseen, J.N. Mitchell, D.A. Smith, M. Mehregany, "High aspect ratio rotary polygon micromotor scanners," *Sensors and Actuators*, A77(1), pp. 73-79, Sept. 1999

[9] A.A. Yasseen, Mitchell, T. Streit, D.A. Smith, M. Mehregany, "A rotary electrostatic micromirror 1x8 optical switch," *IEEE Conf. on Micro Electro Mechanical Systems,* pp. 116-120, Jan. 1998, Heidelberg, Germany

[10] A.P. Lee, A.P. Pisano, "Polysilicon angular vibromotors," *IEEE J. of Micro-electromechanical Sys.*, 1(2), pp. 70-76, Jun. 1992

[11] L. Chu, J. Hetrick, and Y. Gianchandani, "Electro-Thermal Actuators Using Optimized Compliant MicroTransmissions as Rectilinear Motion Amplifiers," *Solid-State Sensors and Actuators Workshop (Hilton Head '00),* Hilton Head Island, South Carolina, June '00

[12] M.-H. Kiang, O. Solgaard, K.Y. Lau, R.S. Muller, "Electrostatic combdrive-actuated micromirrors for laser-beam scanning and positioning," *IEEE J. Microelectromechanical Sys*, 7(1), pp. 27-37, Mar. '98

[13] M. Pai, N.C. Tien, "Current-controlled bi-directional electrothermally actuated vibromotor," *IEEE International Conference on Solid-State Sensors and Actuators (Transducers '99),* pp. 1764-7, Jun. 1999, Sendai, Japan

LIST OF TABLES AND FIGURES

Table I: Dimensions of p^{++} Si rotary output actuators in μm and radians. L1=L2≈L3, θ1=0.1 rad, and θ2=0.2 rad. L3 is the length of the push rods. All devices are 6.5 μm thick, except RJ3, which is 11.0 μm thick. The load beam is 250 μm long, and 3.15 μm wide; D = diagonal placement; Y = placement across the Y actuator drive shaft alone.

Name	L	W1	W2	θ3	Load
R3	1000	4.3	2.3	0	none
R5	500	5.5	5.5	0	D
R6	500	5.2	3.2	0.2	Y
RJ3	500	5.7	6.7	0.2	none

Table II: Measurement results of electroplated Ni inchworms listing device thickness, peak displacement achieved, calculated stiffness of the spring at the base of the shank, and actuation method (for which P=voltage pulse).

Device Type	Thick-ness (μm)	**Displ. (μm)**	K_{sp} (N/m)	Actuation Method
I11	9.0	**40**	0.51	DC: 1V
I33	14.0	**56**	0.895	P: 24 ms, 0.8V
I100	8.4	**32**	5.33	DC: 1V
IL1	11.0	**104**	1.96	P: 24 ms, 1.2V
IL4	9.8	**48**	1.73	P: 38 ms, 1.2V

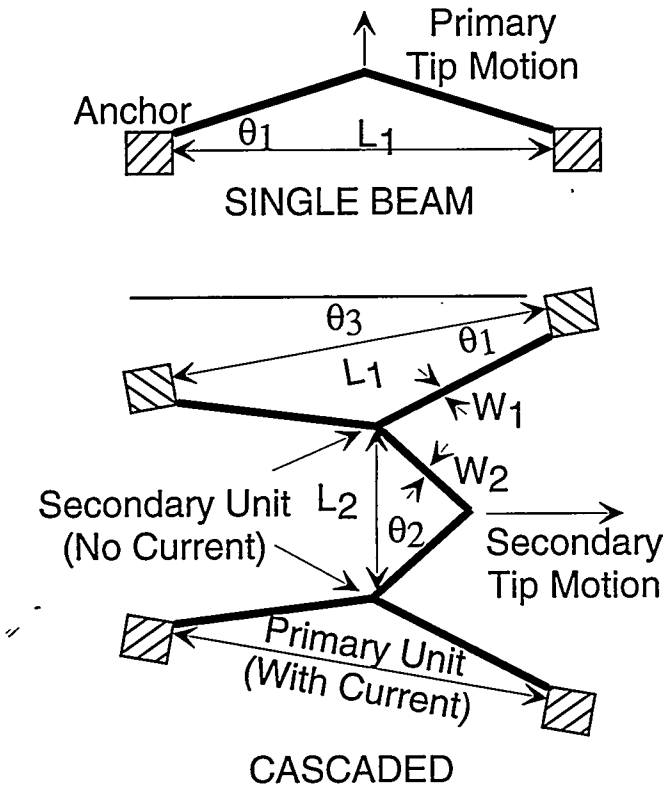

Fig. 1 The basic unit of the bent-beam thermal actuator (left), and a cascaded device (right).

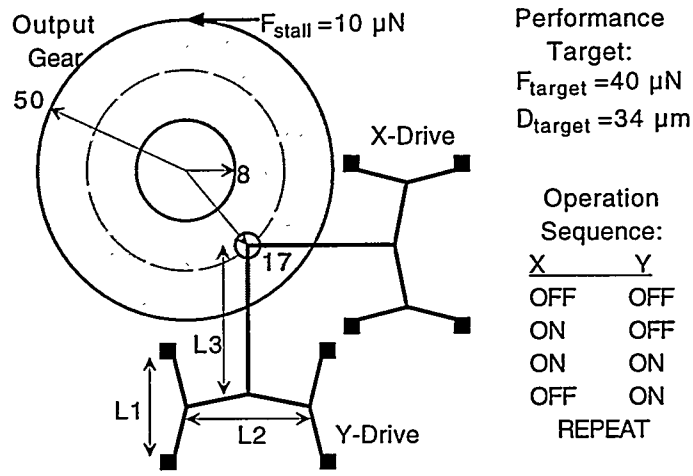

Fig. 2: Schematic (not to scale) of a rotary actuator based on orthogonal cascaded bent-beam elements for a gear of 50 μm radius.

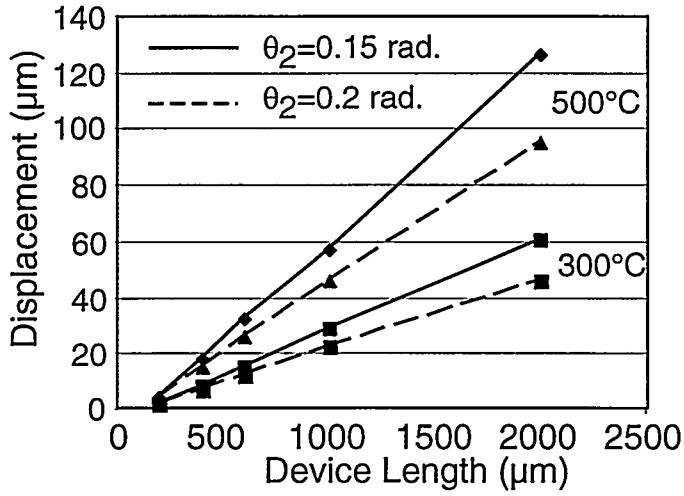

Fig. 3: Non-linear FEA of an orthogonal pair of cascaded Si actuators with one axis actuated. Dimensions: W1=6 μm, W2=W3=4 μm, θ1=0.1rad., H=4.5 μm, and L1=L2=L3.

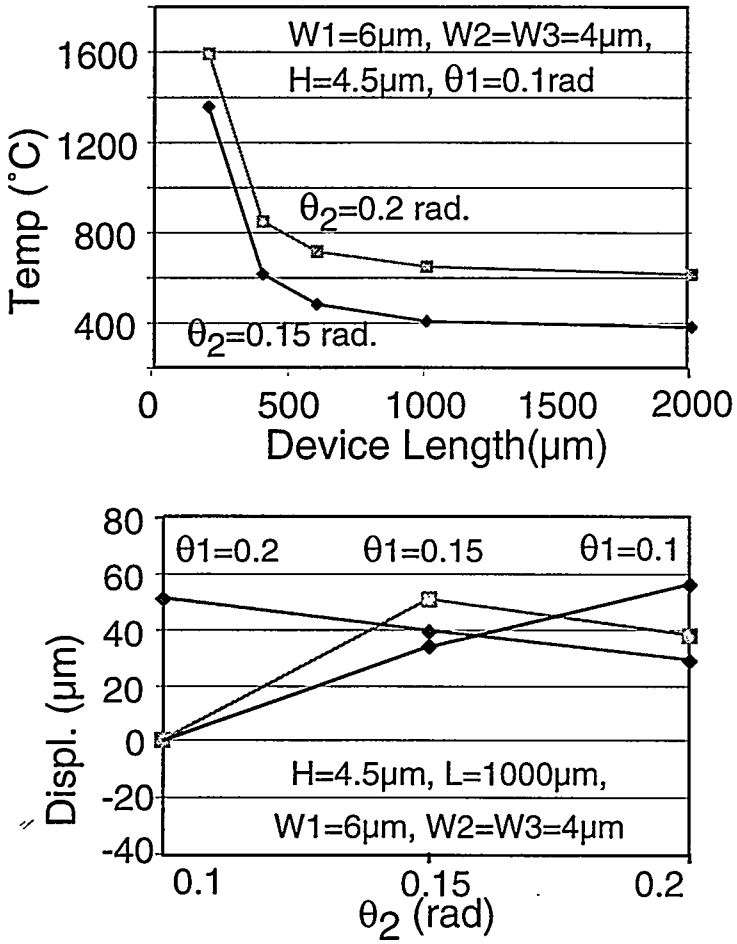

Fig. 4: FEA of orthogonal pairs, with 40 μN external loading force, and non-linear expansion of Si. (a-upper) The maximum average operating temperature that can be achieved before out-of-plane buckling occurs; (b-lower) Lateral displacements that can be achieved before in-plane buckling occurs.

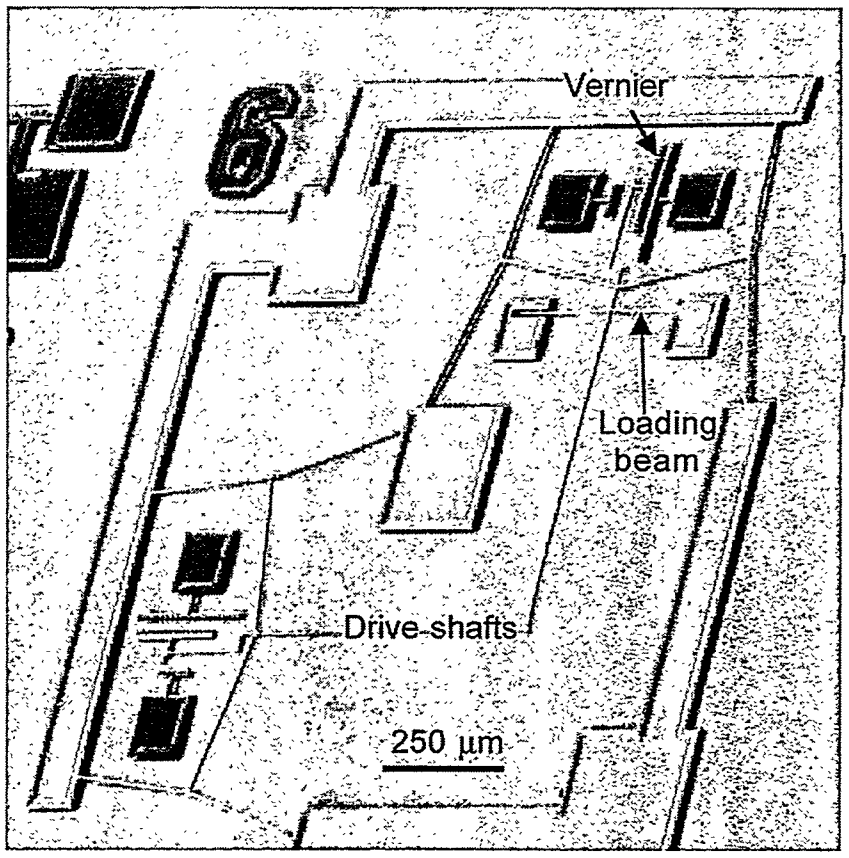

Fig. 5: SEM image of a orthogonal pair of cascaded actuators fabricated from p^{++} Si using the dissolved wafer process.

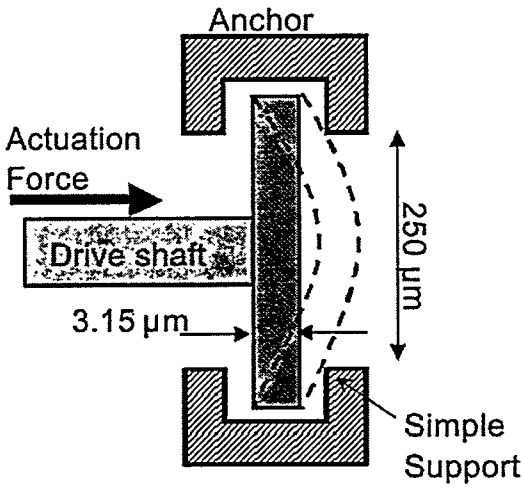

Fig. 6: Schematic of a loading beam used to measure output force available from an actuator.

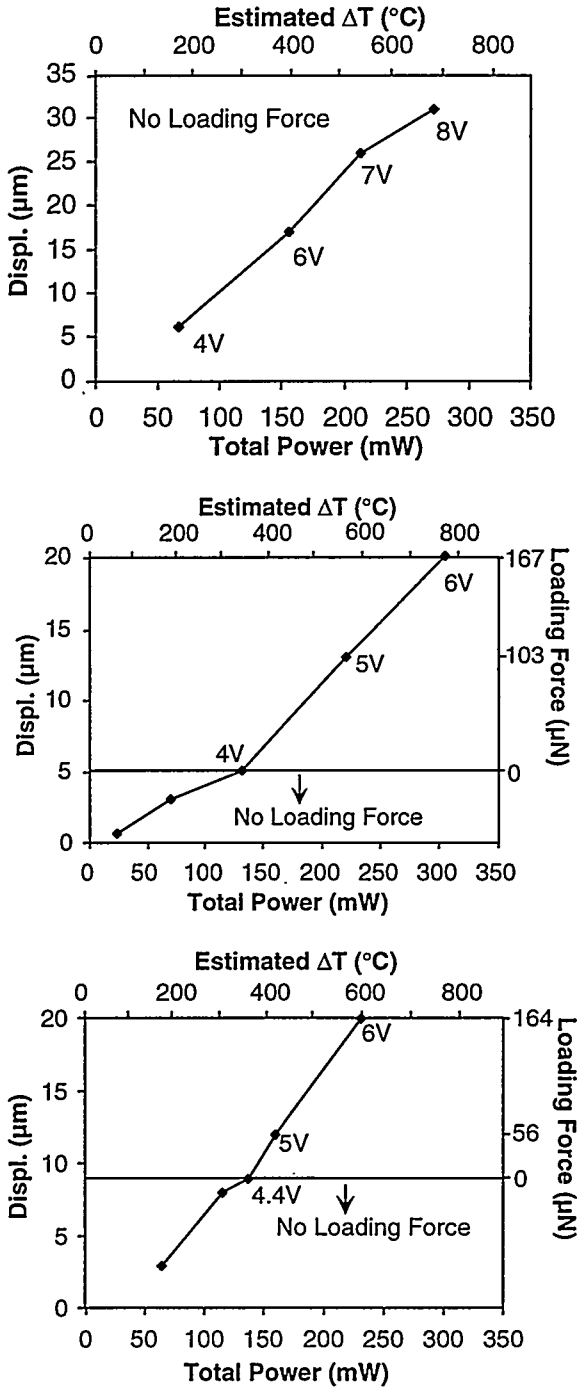

Fig. 7: (a: top–c: bottom) Displacement measurements of p^{++} Si rotary actuators R3, R5, and R6, respectively (Table I). In all cases the X and Y actuators were activated together.

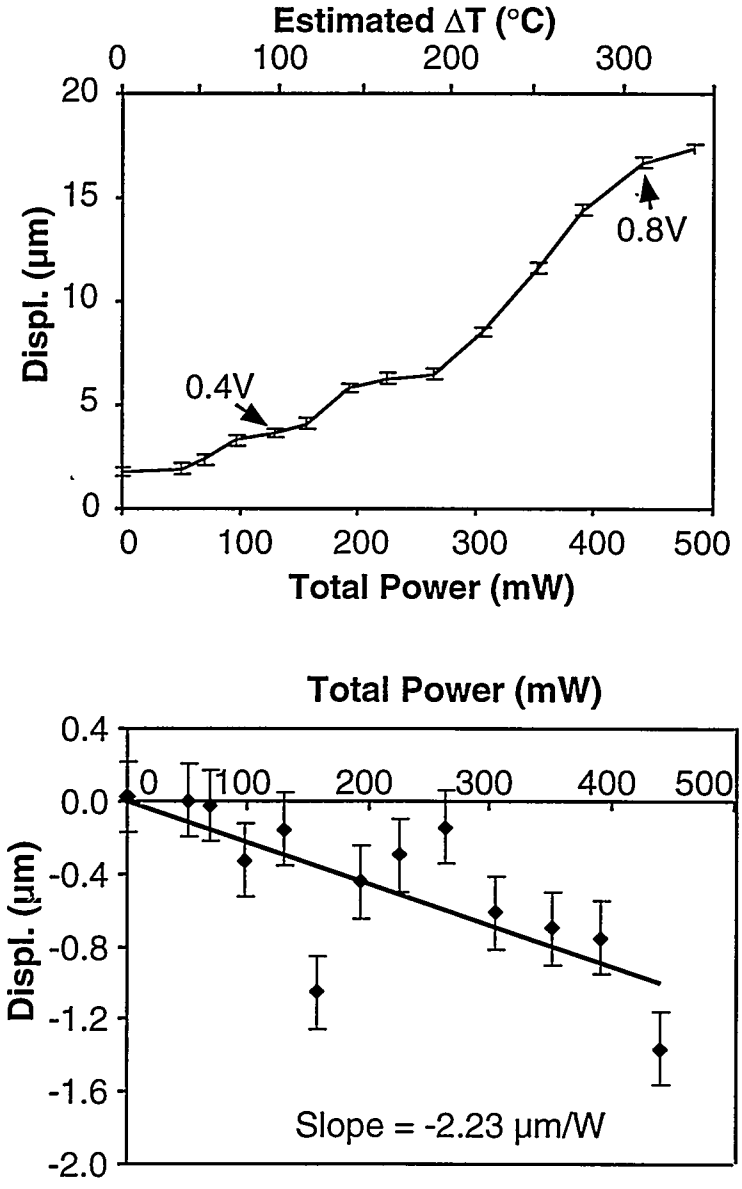

Fig. 8: Measured results of electroplated Ni rotary actuator RJ3 (Table I) with only one axis actuated: (a-upper) the forward displacement of the actuated axis; and (b-lower) a small backward displacement along the orthogonal axis which can be easily compensated.

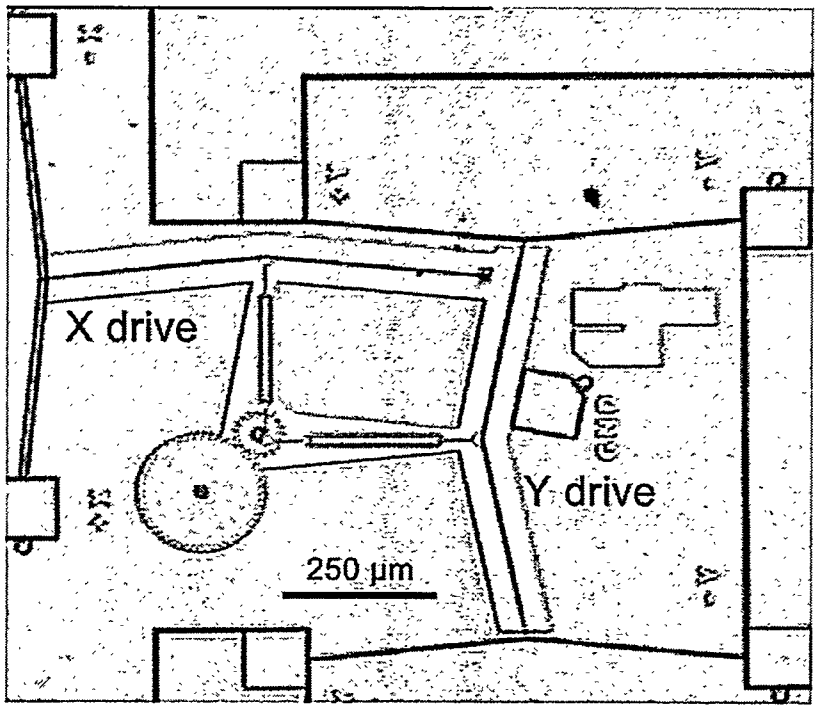

Fig. 9: An optical micrograph of a modified orthogonal-pair actuator fabricated in the Sandia SUMMiT™ process using polysilicon as the structural material.

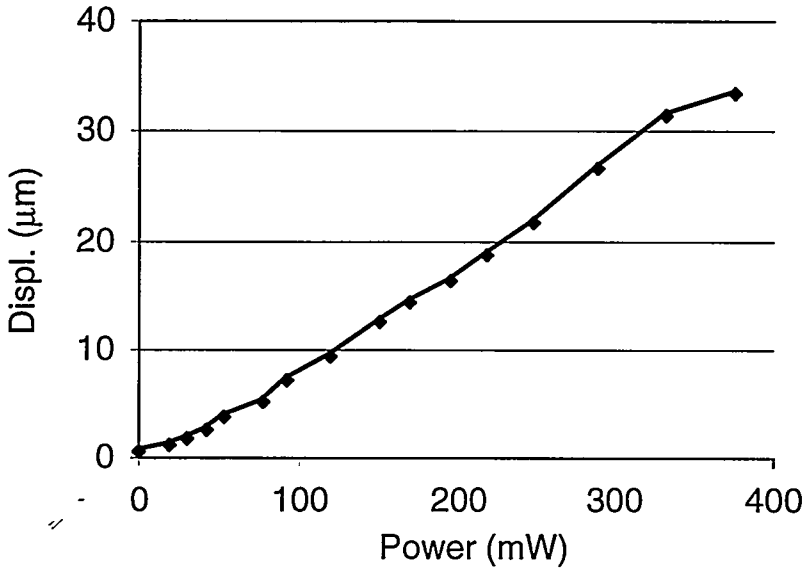

Fig. 10: Measured response of an isolated an unloaded Y-drive of the rotary actuator shown in Fig. 9. The maximum drive voltage used for this curve was 15 V.

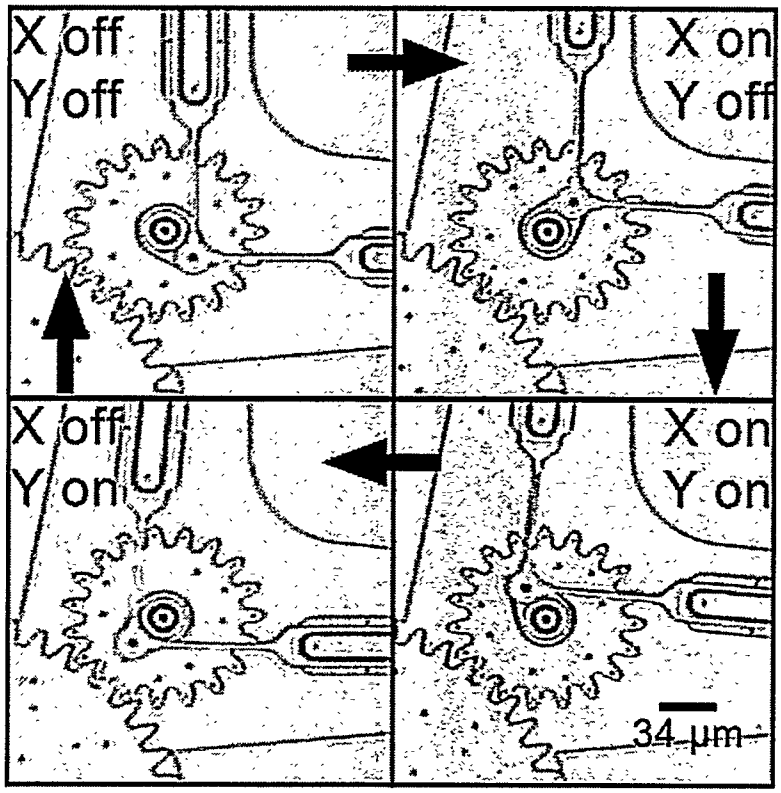

Fig. 11: Time sequenced operation of the rotary engine shown in Fig. 9.

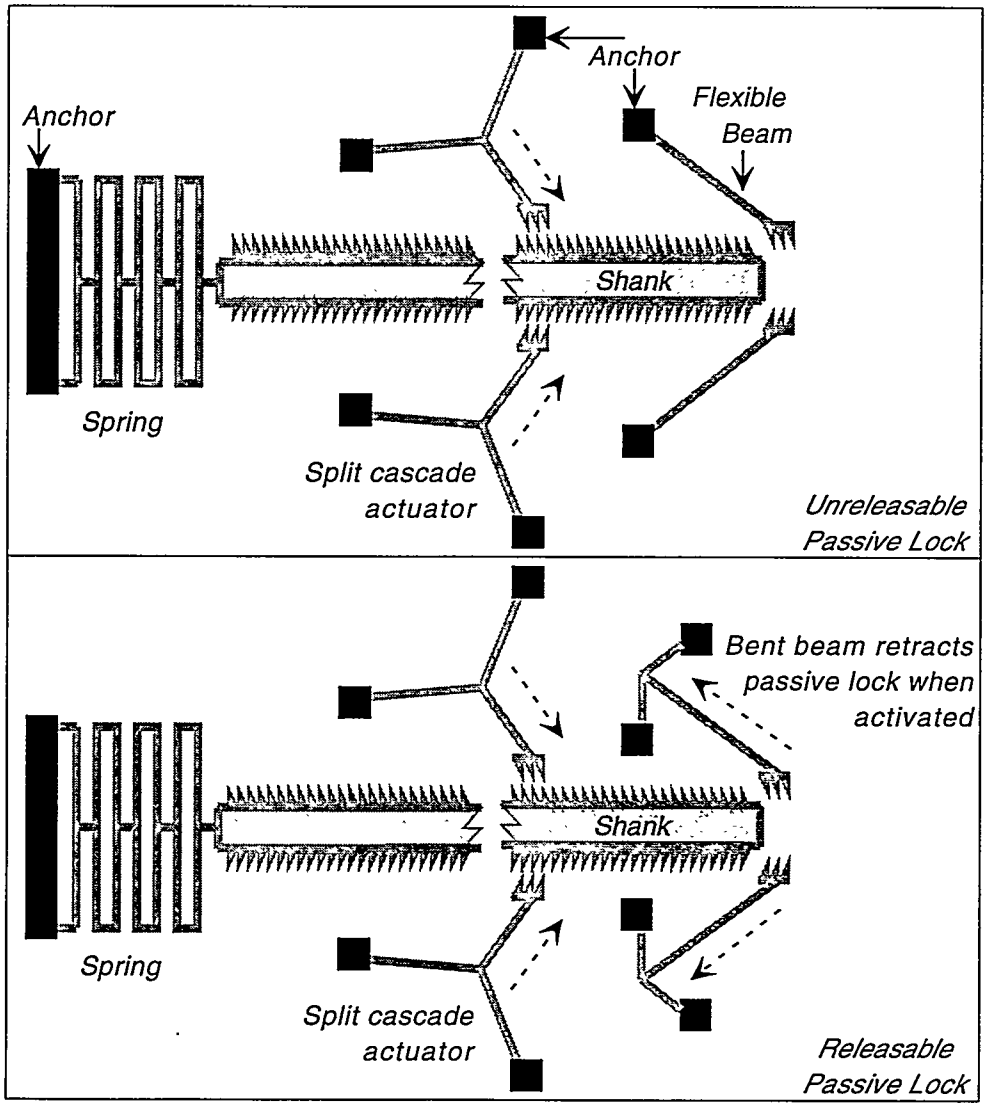

Fig. 12: (a-upper) An inchworm actuator with passive lock that will prevent the pull-back of the shank when power to the actuator is turned off; (b-lower) An inchworm with a retractable passive lock.

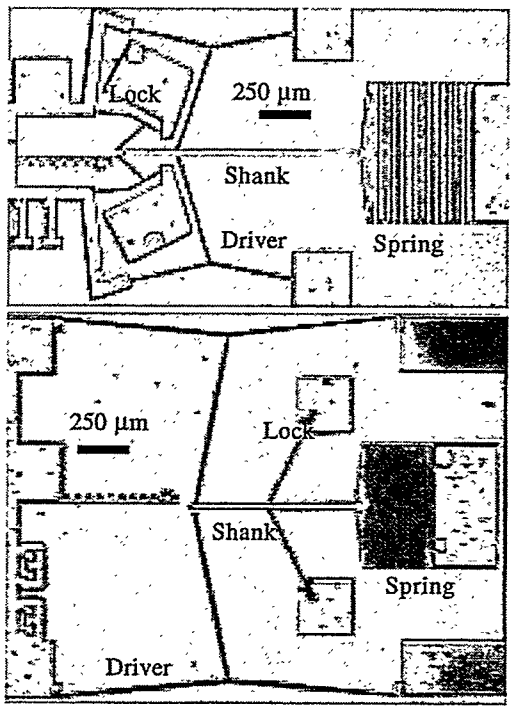

Fig. 13: Optical micrographs of inchworms I11 (upper) and I33 (lower).

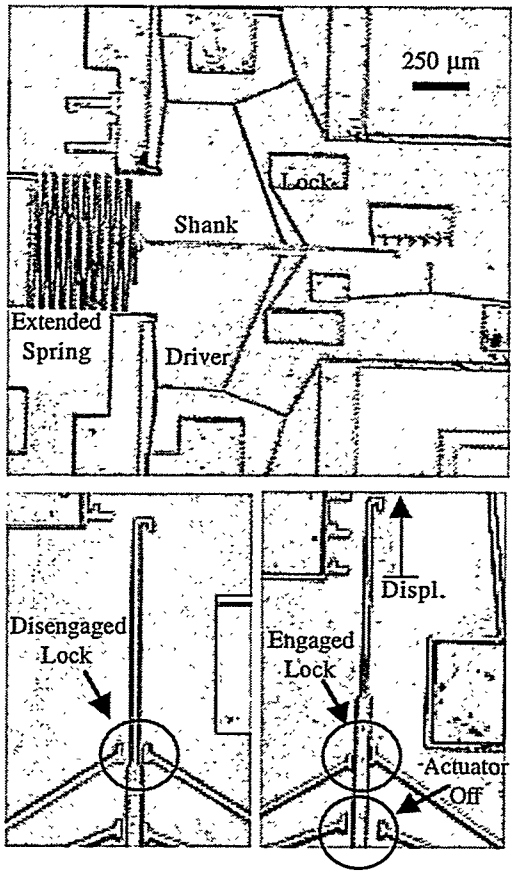

Fig. 14: Optical micrographs showing a locked displacement of 104 µm in inchworm IL1 (upper) and close-up images of the shank before actuation (lower left), and after actuation (lower right).